

## Intrinsic Quantum Anomalous Hall Effect with In-Plane Magnetization: Searching Rule and Material Prediction

Zhao Liu,<sup>1</sup> Gan Zhao,<sup>1</sup> Bing Liu,<sup>1</sup> Z. F. Wang,<sup>1,\*</sup> Jinlong Yang,<sup>2,†</sup> and Feng Liu<sup>3,4,‡</sup>

<sup>1</sup>Hefei National Laboratory for Physical Sciences at the Microscale,  
CAS Key Laboratory of Strongly-Coupled Quantum Matter Physics,  
University of Science and Technology of China, Hefei, Anhui 230026, China

<sup>2</sup>Hefei National Laboratory for Physical Sciences at the Microscale,  
Synergetic Innovation Center of Quantum Information and Quantum Physics,  
University of Science and Technology of China, Hefei, Anhui 230026, China

<sup>3</sup>Department of Materials Science and Engineering, University of Utah, Salt Lake City, Utah 84112, USA

<sup>4</sup>Collaborative Innovation Center of Quantum Matter, Beijing 100084, China



(Received 17 July 2018; published 13 December 2018)

So far, most theoretically predicted and experimentally confirmed quantum anomalous Hall effects (QAHEs) are limited in two-dimensional (2D) materials with out-of-plane magnetization. In this Letter, starting from 2D nodal-line semimetal, a general rule for searching QAHE with in-plane magnetization is mapped out. Because of spin-orbital coupling, we found that the magnetization will prefer an in-plane orientation if the orbital of degenerate nodal-line states at the Fermi level have the same absolute value of magnetic quantum number. Moreover, depending on the broken or conserved mirror symmetry, either a QAHE or 2D semimetal can be realized. Based on first principles calculations, we further predict a real material of monolayer LaCl to be an intrinsic QAHE with in-plane magnetization. By tuning the directions of in-plane magnetization, the QAHE in LaCl demonstrates a threefold rotational symmetry with a Chern number of either +1 or -1, and the transition point is characterized by a 2D semimetal phase. All these features are quantitatively reproduced by tight-binding model calculations, revealing the underlying physics clearly. Our results greatly extend the scope for material classes of QAHE and hence stimulate immediate experimental interest.

DOI: [10.1103/PhysRevLett.121.246401](https://doi.org/10.1103/PhysRevLett.121.246401)

As the last piece of puzzle in the Hall family, the quantum anomalous Hall effect (QAHE) has been intensively studied in recent years [1–4]. There are two essential ingredients for realizing QAHE. One is ferromagnetism, which can be the intrinsic magnetism of a material [5] or extrinsic magnetism induced by magnetic doping [6]. The other is spin-orbital coupling (SOC), which induces a nontrivial topological phase. Theoretically, plenty of materials have been predicted to host QAHE [5–14]. Experimentally, however, only one magnetically doped topological insulator is confirmed to host QAHE [15,16]. In all the prior works, there is one default assumption, namely, the ferromagnetism must have an out-of-plane magnetization. This is similar to the quantum Hall effect that can only be observed in a perpendicular magnetic field [17].

Physically, the out-of-plane magnetization is only a sufficient, but not a necessary, condition for QAHE. In 2013, based on 2D point group symmetry analysis, Liu *et al.* theoretically verified that the in-plane magnetization can also induce QAHE, once it breaks all the mirror symmetries [18]. Later on, Qiao *et al.* proposed two other buckled hexagonal lattices [19,20] to achieve the same goal. However, most proposals are toy model calculations, and the underlying

relationship between magnetic anisotropy and local electronic structure has not been established. To the best of our knowledge, it is still unclear how to search QAHE in a real ferromagnetic material with in-plane magnetization. In this Letter, we will fill this outstanding gap by introducing a general searching rule and then predicting a real material of monolayer LaCl to realize an intrinsic QAHE with the in-plane magnetization through first principles calculations.

The proposed searching rule for QAHE with in-plane magnetization is schematically shown in Fig. 1. Without losing the generality, we start from a 2D nodal-line semimetal, which breaks the time-reversal symmetry but conserves the inversion symmetry, as shown in the left part of Fig. 1. The 2D nodal-line semimetal is generated by the band crossing between two inverted bands with opposite spins. Following the work of Whangbo *et al.* [21], we use the perturbation theory, in which SOC Hamiltonian is taken as a perturbation for the frontier orbitals at the Fermi level to reveal the underlying relationship between magnetic anisotropy and nodal line [22]. As summarized in Table I, one can see that the magnetic anisotropy is directly linked with the orbital components. If the absolute value of magnetic quantum number  $|L_z|$  for two degenerate nodal-line states

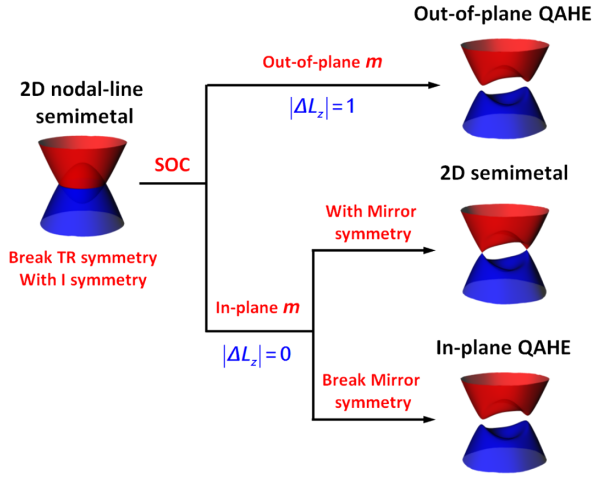


FIG. 1. Schematic rule for searching QAHE with in-plane magnetization. Different topological phases are determined by the direction of magnetization, mirror symmetry, and SOC.

satisfies  $|\Delta L_z| = 0$  or  $|\Delta L_z| = 1$ , the magnetization will prefer the in-plane or out-of-plane direction, respectively, as shown in the middle part of Fig. 1. Therefore, our results provide a guideline to search and design 2D materials with in-plane magnetization through orbital engineering. Furthermore, SOC will drive the 2D nodal-line semimetal into three different topological phases, as shown in the right part of Fig. 1. In 2D point group, the out-of-plane magnetization will break all mirror symmetries [18], inducing a normal QAHE as expected. However, the in-plane magnetization can induce two different phases. In case one, if certain mirror symmetry survives under the in-plane magnetization, the nodal line is degraded into a pair of points protected by the conserved mirror symmetry, inducing a 2D semimetal. In case two, if all in-plane mirror symmetries are broken under the in-plane magnetization, it induces an unexpected QAHE with the in-plane magnetization. The above searching rule indicates that we can use orbital components and lattice symmetries as two screening factors to discover QAHE with in-plane magnetization.

Given the search rule, next we discuss its realization in a real material of monolayer LaCl. The crystal structure of bulk LaCl is shown in Figs. 2(a) and 2(b) (inset). It is an

TABLE I. Preferred direction of magnetization predicted by  $|\Delta L_z|$  and SOC-allowed interaction between two degenerate nodal-line states with opposite spins.

Magnetization	Requirement	Degenerate states
In-plane $\perp z$	$ \Delta L_z  = 0$	$xz$ and $yz$ $xy$ and $x^2 - y^2$ $x$ and $y$
Out-of-plane $\parallel z$	$ \Delta L_z  = 1$	$z^2$ and $\{xz, yz\}$ $\{xz, yz\}$ and $\{xy, x^2 - y^2\}$ $z$ and $\{x, y\}$

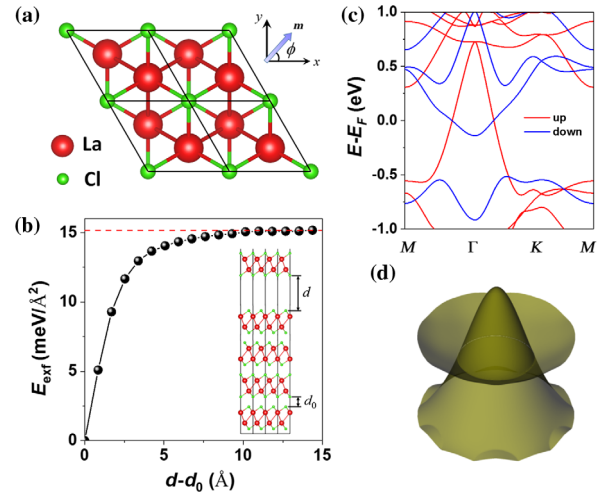


FIG. 2. (a) Top view of monolayer LaCl and angle of in-plane magnetization. (b) Exfoliation energy of monolayer LaCl. Inset is side view of bulk LaCl and interlayer distance. (c) Spin-polarized ferromagnetic band structure of monolayer LaCl without SOC. Red and blue colors denote spin-up and spin-down bands, respectively. (d) 3D band around  $\Gamma$  point near the Fermi level in (c).

*ABC* stacked layer structure, and each layer has two inequivalent La atoms forming a buckled hexagonal lattice [23]. The vertical distance between adjacent layers is  $d_0 = 2.81 \text{ \AA}$ , indicating a weak van der Waals interaction. The exfoliation energy is calculated by a slab model with five LaCl layers [24]. As shown in Fig. 2(b), the converged exfoliation energy is  $\sim 15 \text{ meV/\AA}^2$ , which is even smaller than that of graphene ( $\sim 21 \text{ meV/\AA}^2$ ) and H-MoS<sub>2</sub> ( $\sim 18 \text{ meV/\AA}^2$ ) [24], demonstrating the feasibility to obtain monolayer LaCl through mechanical exfoliation. Furthermore, the stability of monolayer LaCl is confirmed by both phonon calculations and molecular dynamics simulations, as shown in Fig. S1 of the Supplemental Material [22].

To reveal the magnetic ground state of monolayer LaCl, we have carefully checked its spin orientations for both in-plane and out-of-plane configurations. We found that the ferromagnetic state with in-plane magnetization has the lowest energy, as shown in Figs. S2 and S3 of the Supplemental Material [22]. This is consistent with the results reported for bulk LaCl recently [25]. Here, the magnetic anisotropic energy (MAE) ( $\sim 0.15 \text{ meV/La}$ ) is comparable to that in monolayer CrI<sub>3</sub> [26,27], but much larger than that in pure magnetic metals [28]. However, the MAE becomes indistinguishable for in-plane magnetization with different angles ( $\phi$ ), as shown in Fig. S4 of the Supplemental Material [22]. To get a deep understanding about this phenomenon, the spin-polarized band structure of monolayer LaCl without SOC is calculated, as shown in Fig. 2(c). The two inverted bands with opposite spins are crossing at the Fermi level, demonstrating a 2D nodal-line semimetal [see also Fig. 2(d)].

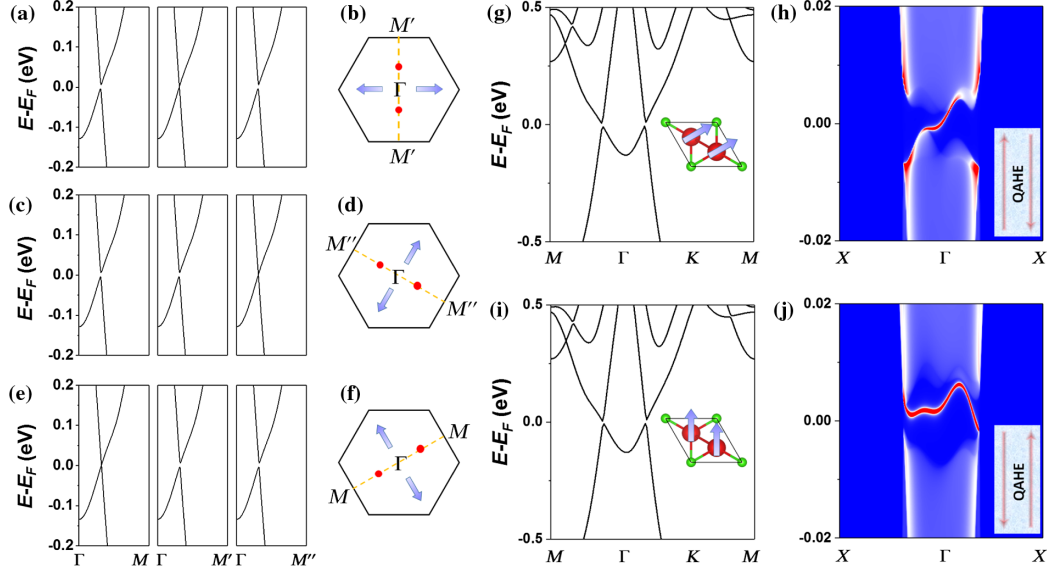


FIG. 3. (a) Band structure of monolayer LaCl with SOC for in-plane magnetization along  $\phi = 0^\circ/180^\circ$ . (b) Schematic two degenerate points (red dot) on the mirror plane (dashed orange line) for in-plane magnetization (blue arrow) perpendicular to the mirror plane in (a). (c)–(f) are the same as (a),(b), but for in-plane magnetization along  $\phi = 60^\circ/240^\circ$  and  $120^\circ/300^\circ$ , respectively. (g) Band structure of monolayer LaCl with SOC for in-plane magnetization along  $\phi = 30^\circ$ , as denoted by the inset arrows. (h) 1D topological edge state for (g), showing QAHE with in-plane magnetization. The inset is schematic propagating direction for left and right edge states. (i),(j) are the same as (g),(h), but for in-plane magnetization along  $\phi = 90^\circ$ .

The orbital-projected bands are shown in Fig. S5 of the Supplemental Material [22]. The spin-up and spin-down bands are mainly  $d_{xy}$ ,  $d_{x^2-y^2}$ , and  $d_{z^2}$ ,  $d_{xy}$ ,  $d_{x^2-y^2}$  orbitals, respectively. Along the nodal line, SOC only allows interaction between degenerate states with opposite spins satisfying  $|\Delta L_z| = 0$  or 1 [22]. Because  $L_z = 0$  for  $d_{z^2}$  and  $L_z = \pm 2$  for  $\{d_{xy}, d_{x^2-y^2}\}$ , the SOC-allowed interaction will be between  $d_{xy}$  and  $d_{x^2-y^2}$ . From Table I, one can see that  $|\Delta L_z| = 0$  prefers the in-plane magnetization, which is consistent with our MAE calculations. Additionally, the estimated Curie temperature for monolayer LaCl is  $\sim 22$  K, as shown in Fig. S6 of the Supplemental Material [22], indicating a low temperature of ferromagnetism.

While turning on SOC, the 2D nodal-line semimetal can be driven into two different phases, depending on the direction of in-plane magnetization, as shown in Fig. 3. The monolayer LaCl has three mirror planes, which are along  $\Gamma$ - $M$ ,  $\Gamma$ - $M'$ , and  $\Gamma$ - $M''$ , as shown in Figs. 3(b), 3(d), and 3(f), respectively. If the mirror plane is perpendicular to the in-plane magnetization, the mirror symmetry will be conserved [18–20]. Otherwise, the mirror symmetry will be broken. Because the mirror symmetry can guarantee a twofold degeneracy, this indicates that SOC can degrade nodal line into a pair of degenerate points sitting on the mirror plane that is perpendicular to the in-plane magnetization. From our first principles calculations, actually, this degraded 2D semimetal phase is revealed, as shown in Figs. 3(a)–3(f). On the other hand, if the in-plane magnetization is not along the above specific directions, all

mirror symmetries are broken. As shown in Figs. 3(g) and 3(i), a global SOC gap ( $\sim 4$  meV) is opened along the nodal line for in-plane magnetization along  $\phi = 30^\circ$  and  $90^\circ$ , respectively. Clearly, the bulk bands are almost the same for these two configurations. The corresponding 1D topological edge state is shown in Figs. 3(h) and 3(j), respectively. Within the energy window of SOC gap, each edge has one edge state connecting the valence and conduction band, demonstrating the characterized feature of QAHE. However, the edge state has an opposite group velocity on the same edge for these two configurations. This indicates that the propagating direction of dissipationless edge current can be controlled by the direction of in-plane magnetization. To further identify the above QAHE, we have also done more accurate hybrid functional calculations, and a similar topological edge state is observed, as shown in Fig. S7 of the Supplemental Material [22]. Therefore, our predicted QAHE with in-plane magnetization is validated, which does not depend on the calculation methods.

To map out the angle dependence of QAHE with in-plane magnetization, 1D edge states are further calculated for in-plane magnetization with different directions, as shown in Fig. S8 of the Supplemental Material [22]. For the same edge, the edge state will reverse its propagating direction on the interval of  $60^\circ$ . The topology can also be identified by Berry curvature (Chern number) calculations. As shown in Figs. 4(a)–4(f) and Fig. S9 of the Supplemental Material [22], there is a periodic jumping of Chern number between  $+1$  and  $-1$  on the interval of  $60^\circ$ .

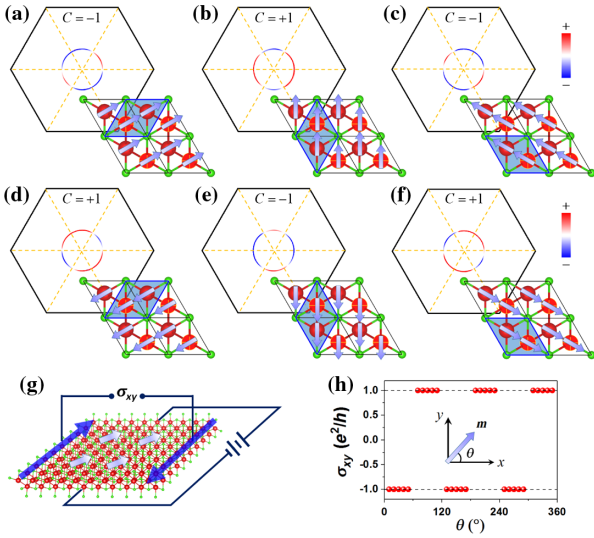


FIG. 4. (a)–(f) Berry curvature and Chern number of monolayer LaCl for in-plane magnetization along  $\phi = 30^\circ, 90^\circ, 150^\circ, 210^\circ, 270^\circ,$  and  $330^\circ$ , respectively. The arrow denotes direction of magnetization, and the shadow region highlights unit cell chosen for different configurations. (g) Schematic QAHE measurement by varying the direction of in-plane magnetization. (h) Quantized Hall conductivity vs direction of in-plane magnetization.

Such an anisotropic QAHE is physically rooted in the lattice symmetry of monolayer LaCl. It is well known that the sign of Chern number is determined by the relative spin orientation. If the spin reverses its direction, the Chern number will change its sign. Therefore, this explains why  $\phi = 30^\circ$  and  $210^\circ$  [Figs. 4(a) and 4(d)],  $\phi = 90^\circ$  and  $270^\circ$  [Figs. 4(b) and 4(e)],  $\phi = 150^\circ$  and  $330^\circ$  [Figs. 4(c) and 4(f)] have the opposite Chern number. Additionally, using the shadow unit cells in Figs. 4(a)–4(f) to guide the eye, one can see that monolayer LaCl with in-plane magnetization has three equivalent configurations by rotating  $120^\circ$  and  $240^\circ$ , respectively. Therefore,  $\phi = 30^\circ, 150^\circ,$  and  $270^\circ$  [Figs. 4(a), 4(c), and 4(e)] have one Chern number, whereas  $\phi = 90^\circ, 210^\circ,$  and  $330^\circ$  [Figs. 4(b), 4(d), and 4(f)] have the other Chern number. The reason for Chern number changing every  $60^\circ$  can also be explained in the same way. For example, if the shadowed unit cell in Fig. 4(a) rotates anticlockwise  $60^\circ$  and then makes an inversion operation, its atomic structure will be the same as that of in Fig. 4(b), but its spin direction will be opposite to that in Fig. 4(b). Consequently,  $\phi = 30^\circ$  and  $90^\circ$  [Figs. 4(a) and 4(b)] have an opposite Chern number. By continuously rotating the in-plane magnetization, the Hall conductivity can be measured, as shown schematically in Fig. 4(g). The angle-dependent quantized Hall conductivity is shown in Fig. 4(h), demonstrating a  $120^\circ$  symmetry. Such features are absent in QAHE with out-of-plane magnetization.

Last, we present a tight-binding (TB) model calculation for monolayer LaCl to better understand QAHE with in-plane magnetization. Without magnetization and SOC, the

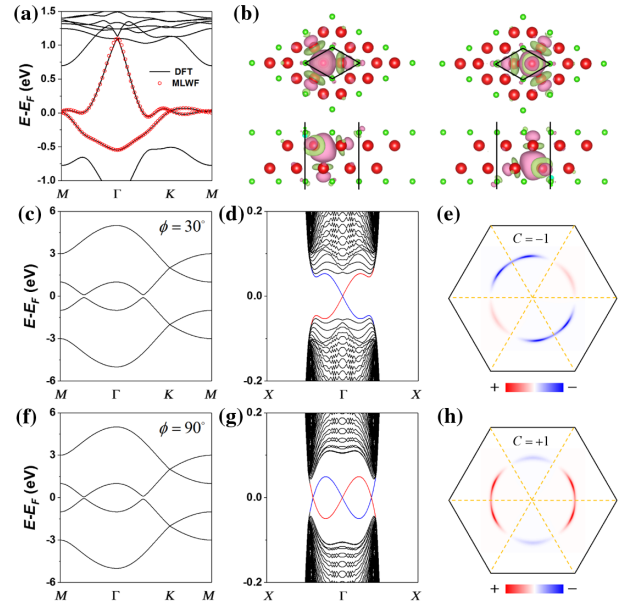


FIG. 5. (a) DFT and Wannier fitted band structure of monolayer LaCl without magnetization and SOC. (b) Top and side views of two fitted WFs. (c) TB band structure with in-plane magnetization along  $\phi = 30^\circ$ . (d) 1D ribbon band structure for (c). Red and blue colors denote left and right edge states, respectively. (e) Berry curvature and Chern number for (c). (f)–(h) are the same as (c)–(e), but for in-plane magnetization along  $\phi = 90^\circ$ . The TB parameters are  $t = 1.0$  eV,  $\lambda_I = 0.03$  eV,  $\lambda_R = -0.03$  eV, and  $t_M = -2.0$  eV.

band structure of monolayer LaCl is shown in Fig. 5(a). Comparing to Fig. 2(c), one can see that the nodal line is generated by spin splitting of two bands near the Fermi level, which can be well fitted by the maximally localized Wannier functions (WF) [29,30]. The WF shape can be considered as a summation of four  $d_{z^2}$  orbitals, and WF center is inside the tetrahedron surrounded by four La atoms, forming a buckled 2D hexagonal lattice, as shown in Fig. 5(b). These results inspire us to construct a four-band TB Hamiltonian as [19,22,31]

$$H = -t \sum_{\langle i,j \rangle} c_i^\dagger c_j + i\lambda_I \sum_{\langle\langle i,j \rangle\rangle} v_{ij} c_i^\dagger s_z c_j - i\lambda_R \sum_{\langle\langle i,j \rangle\rangle} \mu_{ij} c_i^\dagger (\mathbf{s} \times \hat{\mathbf{d}}_{ij}) c_j + t_M \sum_i c_i^\dagger (\mathbf{m} \cdot \mathbf{s}) c_i, \quad (1)$$

where the first term is the nearest-neighbor (NN) hopping, the second term is next NN intrinsic SOC, the third term is next NN intrinsic Rashba SOC, and the fourth term is on-site in-plane magnetization.

The TB band structures without SOC are shown in Fig. S10 of the Supplemental Material [22]. The spin bands are splitting under the weak in-plane magnetization, generating two nodal lines centered at two inequivalent  $K$  points [Fig. S10(d) of the Supplemental Material [22]]. With the increasing strength of in-plane magnetization, two

$K$  centered nodal lines will merge into a  $\Gamma$  centered nodal line [Fig. S10(e) of the Supplemental Material [22]]. If the strength of in-plane magnetization is larger than band width, the nodal line will disappear and two spin bands are separated from each other [Fig. S10(f) of the Supplemental Material [22]]. Such a merging and disappearing of nodal line is accompanied with a topological phase transition [19], and monolayer LaCl is within the nontrivial region, as shown in Fig. S10(e) of the Supplemental Material [22]. Turning on SOC, if the direction of in-plane magnetization is perpendicular to the mirror plane, i.e.,  $\phi = 0^\circ, 60^\circ, 120^\circ, 180^\circ, 240^\circ, 300^\circ$ , the 2D nodal-line semimetal [Fig. S10(e) of the Supplemental Material [22]] will be driven into 2D semimetal with a pair of degenerate points sitting on the mirror plane, as shown in Fig. S11 of the Supplemental Material [22], which is consistent with the results shown in Fig. 3. Next, if the in-plane magnetization deviates from the above six directions, a QAHE is realized. The bulk band, 1D ribbon band, and Berry curvature (Chern number) for  $\phi = 30^\circ$  and  $90^\circ$  are shown in Figs. 5(c)–5(e), and Figs. 5(f)–5(h), respectively. All the features are consistent with those shown in Figs. 3 and 4. Additionally, the QAHE with in-plane magnetization has also shown a  $120^\circ$  symmetry, as shown in Figs. S12 and S13 of the Supplemental Material [22]. Therefore, the topological properties of monolayer LaCl are well reproduced by our TB model.

In conclusion, we establish the underlying relationship between nodal line and magnetic anisotropy, introduce a general rule for searching a QAHE with in-plane magnetization, and predict a real material to realize it. Our results greatly enrich the physics and expand the material family of QAHE, which are expected to draw immediate experimental attention.

This work is supported by NSFC (Grants No. 11774325, No. 21603210, No. 21603205, and No. 21688102), National Key R&D Program of China (Grants No. 2017YFA0204904 and No. 2016YFA0200604), Anhui Initiative in Quantum Information Technologies (Grant No. AHY090400), Fundamental Research Funds for the Central Universities, and U.S. Department of Energy-Basic Energy Sciences (Award No. DE-FG02-04ER46148). We thank Supercomputing Center at University of Science and Technology of China for providing the computing resources.

\*zfwang15@ustc.edu.cn

†jlyang@ustc.edu.cn

‡fliu@eng.utah.edu

[1] F. D. M. Haldane, *Phys. Rev. Lett.* **61**, 2015 (1988).

[2] K. He, Y. Wang, and Q.-K. Xue, *Nat. Sci. Rev.* **1**, 38 (2014).

- [3] H. Weng, R. Yu, X. Hu, X. Dai, and Z. Fang, *Adv. Phys.* **64**, 227 (2015).
- [4] C.-X. Liu, S.-C. Zhang, and X.-L. Qi, *Annu. Rev. Condens. Matter Phys.* **7**, 301 (2016).
- [5] Z. F. Wang, Z. Liu, and F. Liu, *Phys. Rev. Lett.* **110**, 196801 (2013).
- [6] R. Yu, W. Zhang, H.-J. Zhang, S.-C. Zhang, X. Dai, and Z. Fang, *Science* **329**, 61 (2010).
- [7] Z. Qiao, S. A. Yang, W. Feng, W.-K. Tse, J. Ding, Y. Yao, J. Wang, and Q. Niu, *Phys. Rev. B* **82**, 161414(R) (2010).
- [8] J. Ding, Z. Qiao, W. Feng, Y. Yao, and Q. Niu, *Phys. Rev. B* **84**, 195444 (2011).
- [9] H. Zhang, C. Lazo, S. Blügel, S. Heinze, and Y. Mokrousov, *Phys. Rev. Lett.* **108**, 056802 (2012).
- [10] J. Wang, B. Lian, H. Zhang, Y. Xu, and S.-C. Zhang, *Phys. Rev. Lett.* **111**, 136801 (2013).
- [11] S.-C. Wu, G. Shan, and B. Yan, *Phys. Rev. Lett.* **113**, 256401 (2014).
- [12] K. Dolui, S. Ray, and T. Das, *Phys. Rev. B* **92**, 205133 (2015).
- [13] L. Dong, Y. Kim, D. Er, A. M. Rappe, and V. B. Shenoy, *Phys. Rev. Lett.* **116**, 096601 (2016).
- [14] Z. F. Wang, Z. Liu, J. Yang, and F. Liu, *Phys. Rev. Lett.* **120**, 156406 (2018).
- [15] C.-Z. Chang *et al.*, *Science* **340**, 167 (2013).
- [16] A. J. Bestwick, E. J. Fox, X. Kou, L. Pan, K. L. Wang, and D. Goldhaber-Gordon, *Phys. Rev. Lett.* **114**, 187201 (2015).
- [17] K. von Klitzing, *Rev. Mod. Phys.* **58**, 519 (1986).
- [18] X. Liu, H.-C. Hsu, and C.-X. Liu, *Phys. Rev. Lett.* **111**, 086802 (2013).
- [19] Y. Ren, J. Zeng, X. Deng, F. Yang, H. Pan, and Z. Qiao, *Phys. Rev. B* **94**, 085411 (2016).
- [20] P. Zhong, Y. Ren, Y. Han, L. Zhang, and Z. Qiao, *Phys. Rev. B* **96**, 241103(R) (2017).
- [21] M.-H. Whangbo, E. E. Gordon, H. Xiang, H.-J. Koo, and C. Lee, *Acc. Chem. Res.* **48**, 3080 (2015).
- [22] See Supplementary Material at <http://link.aps.org/supplemental/10.1103/PhysRevLett.121.246401> for theoretical methods and additional first-principles and tight-binding results.
- [23] R. E. Araujo and J. D. Corbett, *Inorg. Chem.* **20**, 3082 (1981).
- [24] J. H. Jung, C.-H. Park, and J. Ihm, *Nano Lett.* **18**, 2759 (2018).
- [25] S. Nie, H. Weng, and F. B. Prinz, arXiv:1803.08486.
- [26] B. Huang *et al.*, *Nature (London)* **546**, 270 (2017).
- [27] J. L. Lado and J. Fernández-Rossier, *2D Mater.* **4**, 035002 (2017).
- [28] S. V. Halilov, A. Ya. Perlov, P. M. Oppeneer, A. N. Yaresko, and V. N. Antonov, *Phys. Rev. B* **57**, 9557 (1998).
- [29] A. A. Mostofi, J. R. Yates, Y.-S. Lee, I. Souza, D. Vanderbilt, and N. Marzari, *Comput. Phys. Commun.* **178**, 685 (2008).
- [30] Z. F. Wang and F. Liu, *Phys. Rev. Lett.* **115**, 026803 (2015).
- [31] C.-C. Liu, H. Jiang, and Y. Yao, *Phys. Rev. B* **84**, 195430 (2011).